ARTICLE

doi:10.1038/nature14415

Sequential cancer mutations in cultured human intestinal stem cells

Jarno Drost[1,2], Richard H. van Jaarsveld[2,3]*, Bas Ponsioen[2,3]*, Cheryl Zimberlin[2,4]*, Ruben van Boxtel[1,2], Arjan Buijs[5], Norman Sachs[1,2], René M. Overmeer[2,3], G. Johan Offerhaus[6], Harry Begthel[1,2], Jeroen Korving[1,2], Marc van de Wetering[1,2,7], Gerald Schwank[1,2], Meike Logtenberg[1,2], Edwin Cuppen[1,2], Hugo J. Snippert[2,3], Jan Paul Medema[2,4], Geert J. P. L. Kops[2,3] & Hans Clevers[1,2]

Crypt stem cells represent the cells of origin for intestinal neoplasia. Both mouse and human intestinal stem cells can be cultured in medium containing the stem-cell-niche factors WNT, R-spondin, epidermal growth factor (EGF) and noggin over long time periods as epithelial organoids that remain genetically and phenotypically stable. Here we utilize CRISPR/Cas9 technology for targeted gene modification of four of the most commonly mutated colorectal cancer genes (*APC*, *P53* (also known as *TP53*), *KRAS* and *SMAD4*) in cultured human intestinal stem cells. Mutant organoids can be selected by removing individual growth factors from the culture medium. Quadruple mutants grow independently of all stem-cell-niche factors and tolerate the presence of the P53 stabilizer nutlin-3. Upon xenotransplantation into mice, quadruple mutants grow as tumours with features of invasive carcinoma. Finally, combined loss of *APC* and *P53* is sufficient for the appearance of extensive aneuploidy, a hallmark of tumour progression.

The adenoma–carcinoma sequence proposes that the sequential acquisition of specific genetic alterations underlies the progression of colorectal cancer (CRC)[1]. Activation of the WNT pathway, most commonly through inactivating mutations in *APC*, initiates the formation of benign polyps. Progression is thought to occur through activating mutations in the EGF receptor (EGFR) pathway and inactivating mutations in the P53 and transforming growth factor (TGF)-β pathways[2]. Recent sequencing efforts have further explored the genomic landscape underlying CRC[3]. A major hurdle in identifying essential driver mutations is that many CRCs have acquired either microsatellite instability or chromosomal instability (CIN), as tumours typically harbour hundreds to thousands of mutations. Using mouse models, $Lgr5^{+}$-intestinal stem cells were identified as cells of origin for intestinal neoplasia and were shown to fuel effective tumour growth[4–6]. A recent study has shown that deregulation (by retroviral expression of short hairpin RNAs (shRNAs) or cDNA) of *APC*, *P53*, *KRAS* and *SMAD4* is sufficient for transformation of cultured mouse colon into tumours with adenocarcinoma-like histology[7]. Of note, the reliance on paracrine growth factors provided by a mesenchymal component in this system does not allow a one-to-one correlation with the individual oncogenic mutations. Comparable human *in vitro* model systems to study tumour initiation and progression have not been developed. We have previously described 'indefinite' three-dimensional stem cell culture systems (organoids) derived from several organs including mouse and human small intestine, colon, pancreas and liver that remain genetically stable[8–13].

Sequential introduction of CRC mutations

We set out to utilize CRISPR/Cas9-mediated genome editing[14–16] to introduce four of the most frequent CRC mutations in human small intestinal organoid stem cell cultures. As the absolute knockout efficiency is low, we made use of functional selection strategies to obtain clonal, mutant organoids. Since loss of *APC* is generally considered to be an early event in CRC[2], we first introduced inactivating mutations in *APC*. As previously described, withdrawal of WNT and R-spondin from the defined culture medium provides a functional selection for *APC* loss[17] (Fig. 1a). Indeed, control-transfected organoids died when seeded in medium lacking WNT and R-spondin (Fig. 1b), whereas transfection of plasmids expressing Cas9 and single guide RNAs (sgRNAs) targeting *APC* in its mutation hotspot region allowed cystic clonal organoids to emerge (Fig. 1b, Extended Data Fig. 1a and Extended Data Table 1a). To obtain clonal cultures, individual organoids were expanded. Genotyping verified the presence of clonal insertions or deletions (indels) at the targeted regions (Extended Data Fig. 1b). Quantitative reverse transcription polymerase chain reaction (qRT–PCR) analysis for the WNT target gene *AXIN2* confirmed the constitutive activity of the WNT pathway, as *AXIN2* messenger RNA levels did not decrease upon WNT/R-spondin withdrawal (Fig. 1c).

Next, we introduced inactivating mutations in *P53* in *APC* knockout (APC^{KO}) intestinal organoids. We made use of nutlin-3 (ref. 18) to select for organoids with a functionally inactive P53 pathway (Fig. 1a). As expected, nutlin-3 stabilized P53 in intestinal organoids and activated transcription of its target gene *P21* (also known as *CDKN1A*) (Fig. 1e). Control sgRNA-transfected APC^{KO} organoids died upon nutlin-3 treatment (Fig. 1d), whereas transfection of plasmids expressing Cas9 and sgRNAs targeting *P53* enabled organoid outgrowth (Fig. 1d, Extended Data Fig. 1a and Extended Data Table 1a). Clonal expansion and genotyping verified the presence of frameshift-inducing indels at the targeted loci (at the start of the DNA-binding domain, thereby yielding an inactive gene product; Extended Data Fig. 1c). Loss of P53 protein expression and P53 pathway inactivity were confirmed by western blot (Fig. 1e).

[1]Hubrecht Institute, Royal Netherlands Academy of Arts and Sciences (KNAW) and UMC Utrecht, 3584CT Utrecht, The Netherlands. [2]Cancer Genomics Netherlands, UMC Utrecht, 3584CG Utrecht, The Netherlands. [3]Molecular Cancer Research, Centre for Molecular Medicine, UMC Utrecht, 3584CG, Utrecht, The Netherlands. [4]Laboratory of Experimental Oncology and Radiobiology, Centre for Experimental Molecular Medicine, AMC, 1105AZ Amsterdam, The Netherlands. [5]Department of Medical Genetics, UMC Utrecht, 3508AB Utrecht, The Netherlands. [6]Department of Pathology, UMC Utrecht, 3584CX Utrecht, The Netherlands. [7]Foundation Hubrecht Organoid Technology (HUB), 3584CT Utrecht, The Netherlands.
*These authors contributed equally to this work.

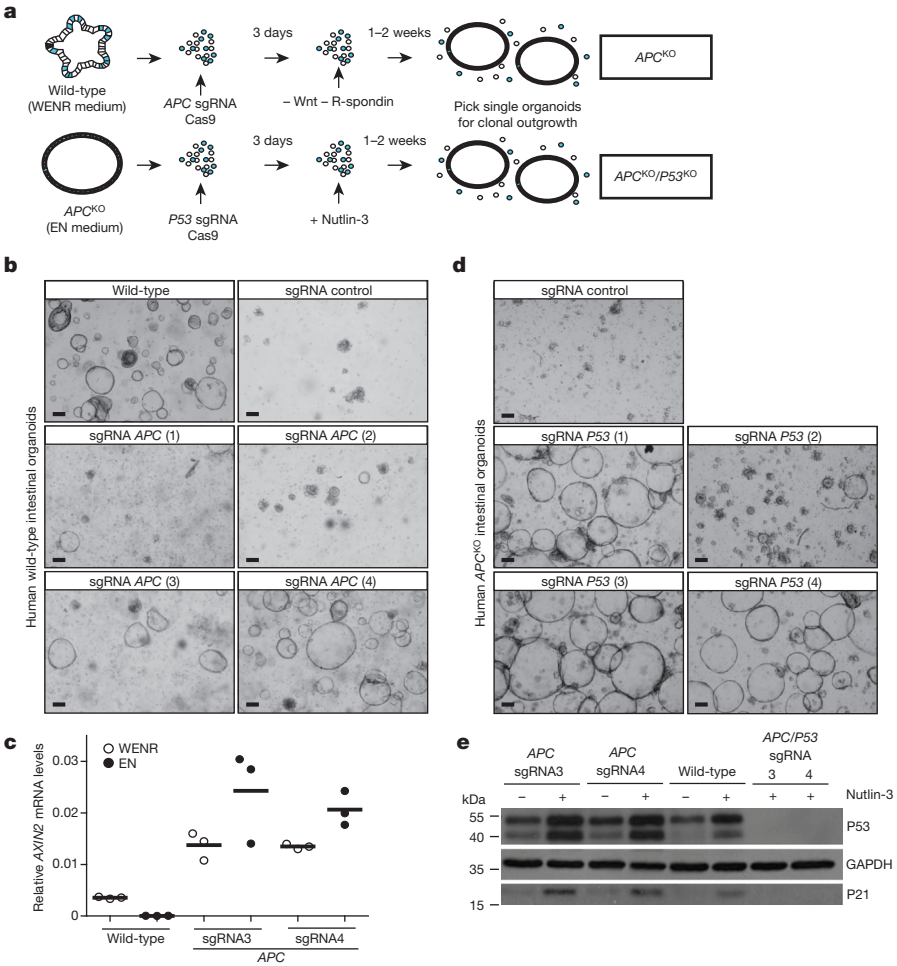

Figure 1 | Inactivation of *APC* and *P53* in human intestinal organoids. **a**, Strategy to generate the indicated mutant lines using CRISPR/Cas9. Blue, stem cells. E, EGF; N, noggin; R, R-spondin; W, WNT. **b**, Wild-type organoids in complete medium (WENR; top left) and transfected with Cas9 and the indicated sgRNAs selected in EN medium (representative pictures from $n = 3$ independent experiments). **c**, qRT–PCR for *AXIN2* in wild-type and APC^{KO} organoids in the presence or absence of WNT/R-spondin. Expression normalized to *GAPDH*. Horizontal bars represent mean of $n = 3$ independent experiments. **d**, APC^{KO} organoids were transfected with Cas9 and the indicated sgRNAs. *P53* mutants were selected in medium with nutlin-3 (representative pictures from $n = 3$ independent experiments). **e**, Western blot analysis of P53 and P21 expression in organoids cultured in the presence/absence of nutlin-3 (representative from $n = 3$ independent experiments). Scale bars, 100 μm.

The most common *KRAS* mutation in CRC results in the expression of constitutively active KRAS(G12D). To introduce this mutation, we designed an oligonucleotide with the oncogenic mutation and two silent mutations to serve as a template for homologous recombination (Fig. 2a). $KRAS^{G12D}$ mutants were selected by withdrawing EGF and adding the EGFR inhibitor gefitinib to the culture medium. Of note, resident Paneth cells produce EGF in organoids[9]. Whereas control-transfected organoids failed to expand in the selection medium, organoids transfected with the oligonucleotide, Cas9 and the *KRAS* sgRNA grew out (Fig. 2b and Extended Data Table 1a). Genotyping of clonally expanded organoids confirmed that the resistant clones harboured the $KRAS^{G12D}$ mutation (Fig. 2c). The two silent mutations were also present in the recombined allele, verifying that the mutations were introduced using the provided template. Although the second *KRAS* allele did not recombine, it was often targeted by Cas9 endonuclease, resulting in a frameshift in the second allele.

Quadruple mutants do not need niche factors

We then set out to introduce combinations of CRC mutations. We used our KRAS(G12D)-expressing organoids to introduce inactivating mutations in *APC*, *P53* and *SMAD4* (Fig. 2d). To select for inactivating mutations in *SMAD4*, an essential downstream component of the TGF-β and bone morphogenetic protein (BMP) pathways, we made use of the dependence of the intestinal organoids on the presence of the BMP pathway inhibitor noggin in the culture medium[9]. Using the described selection procedures, transfection of Cas9 with either *APC* or both *APC* and *P53* sgRNAs yielded $KRAS^{G12D}/APC^{KO}$ and $KRAS^{G12D}/APC^{KO}/P53^{KO}$ organoids, respectively (Fig. 2e, f and Extended Data Fig. 2a, b, e). Transfection of Cas9 together with sgRNAs targeting *APC*, *P53* and *SMAD4* yielded organoids growing in medium lacking EGF, WNT, R-spondin and noggin, to which nutlin-3 was added (Fig. 2e, Extended Data Fig. 2d and Extended Data Table 1a). Clonal expansion and sequencing of the targeted loci in *APC* and *P53* verified frameshift-inducing indels. Sequencing of the targeted exon in *SMAD4* in several different clones revealed a frameshift-inducing deletion in one allele and an in-frame deletion in the other allele (sgRNA 1, P356del; sgRNA 3, V370del) (Extended Data Fig. 2c). Western blot confirmed reduced protein expression in *SMAD4*-mutated organoids (Fig. 2f). As with all sgRNAs, *SMAD4* sgRNAs target the mutation hotspot region, encoding the MH2 domain required for SMAD4 activity[19,20]. Recently, in-frame deletions of SMAD4 P356 and V370 were shown to occur in CRC[21], indicating that in-frame indels at these locations yield an inactive gene product. Using a candidate off-target prediction tool,

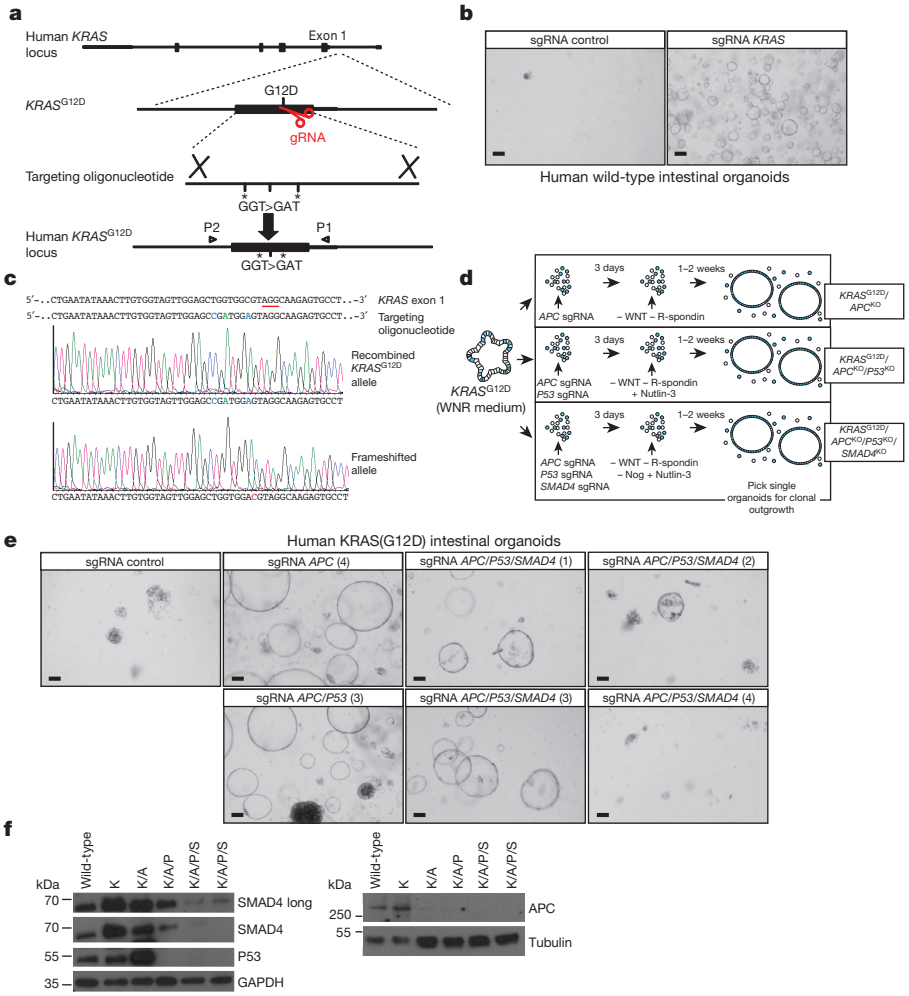

Figure 2 | *KRAS*^{G12D}/*APC*^{KO}/*P53*^{KO}/*SMAD4*^{KO} organoids grow in the absence of stem-cell-niche factors *in vitro*. **a**, Strategy to introduce the *KRAS*^{G12D} mutation. Asterisks indicate silent mutations; arrowheads indicate genotype primers. **b**, Wild-type human intestinal organoids were transfected with Cas9, sgRNA and the oligonucleotide. *KRAS*^{G12D} mutants were selected in medium lacking EGF, with the EGFR inhibitor gefitinib (representative pictures from $n = 3$ independent experiments). **c**, Sequence analysis of the targeted *KRAS* exon. Oncogenic GGT>GAT mutation is indicated in green; silent mutations are in blue; protospacer adjacent motif (PAM) is underlined in red. **d**, Strategy to generate the indicated mutant lines using CRISPR/Cas9. Blue, stem cells. N, noggin (Nog); R, R-spondin; W, WNT. **e**, KRAS(G12D)-expressing organoids were transfected with Cas9 and the indicated sgRNAs (representative pictures from $n = 3$ independent experiments). **f**, Western blot analysis of SMAD4, P53 and APC expression in the indicated organoid lines (representative from $n = 3$ independent experiments). K, *KRAS*^{G12D}; A, *APC*^{KO}; P, *P53*^{KO}; S, *SMAD4*^{KO}. Scale bars, 100 μm.

we detected no lesions of predicted off-target sites for the sgRNAs used to introduce mutation combinations in our human intestinal organoids (Supplementary Table 1). Although this analysis was limited, in combination with the analysis of multiple independent clonal organoids, the results indicated that the observed effects were not due to off-target effects. In conclusion, *KRAS*^{G12D}/*APC*^{KO}/*P53*^{KO}/*SMAD4*^{KO} mutant intestinal organoids can grow in the absence of all stem-cell-niche factors *in vitro* (Extended Data Table 1b).

Quadruple mutants grow as invasive carcinomas

Next, we investigated whether our engineered organoids were tumorigenic *in vivo*. We subcutaneously injected wild-type and all engineered mutant organoid lines into immunodeficient mice. After 8 weeks, some mice injected with *KRAS*^{G12D}/*APC*^{KO}/*P53*^{KO} organoids ('triple'; 3 out of 12 injections) and the majority of mice injected with *KRAS*^{G12D}/*APC*^{KO}/*P53*^{KO}/*SMAD4*^{KO} organoids ('quadruple'; 13 out of 16 injections) developed visible nodules (Extended Data Fig. 4a). Histological analysis confirmed that triple organoids did engraft, but remained small with few proliferating cells and mostly resembled adenomas (Fig. 3a and Extended Data Fig. 4b, c). Quadruple-derived tumours were larger, highly proliferative and all displayed features of invasive carcinoma, including an irregular multi-layered epithelium consisting of tumour cells with increased nuclear–cytoplasmic ratio, pleiomorphic and hyperchromatic nuclei. Invasion of isolated or small aggregates of tumour cells into the stroma was frequently observed (Fig. 3b and Extended Data Fig. 4b, d). The tumour origin was verified using a human-specific cytokeratin antibody (hKRT; Fig. 3 and Extended Data Fig. 4c, d). Thus, introduction of oncogenic mutations in *KRAS*, *APC*, *P53* and *SMAD4* enables normal human intestinal stem cell organoids to grow as tumours with invasive carcinoma features *in vivo* (Extended Data Table 1b). *In vitro*, both triple- and quadruple-mutant organoids exhibited a high proliferation rate, while only quadruple-mutant organoids frequently appeared as solid tumour masses (Extended Data Fig. 5a, c).

Extensive aneuploidy upon *APC* and *P53* loss

To determine whether our engineered mutant organoids acquired CIN, a hallmark of CRC[22], we transduced all human intestinal organoid lines with a fluorescently tagged histone 2B (H2B)-encoding lentivirus. This enabled us to monitor chromosome segregations

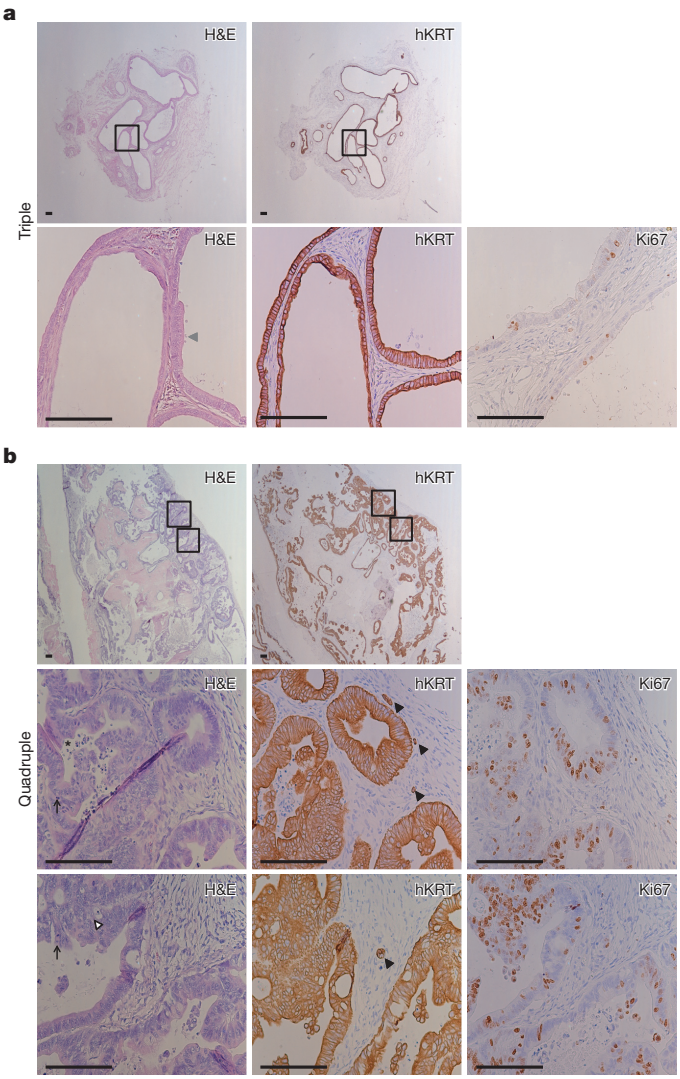

Figure 3 | Quadruple-mutant organoids grow as invasive carcinomas *in vivo*. **a**, Haematoxylin and eosin (H&E; top left, bottom left), hKRT (top right, bottom middle) and Ki67 (bottom right) immunostainings on nodules isolated from triple-mutant-injected mice. Representative pictures of an adenoma with regular glandular structures lined with a blander epithelium that only focally shows a tendency towards stratification (arrowhead), no invasive growth and low proliferative capacity (Ki67). $n = 3$ mice. **b**, As in **a**, but for quadruple-mutant-injected mice. Upper and lower boxed regions in top panels correspond to regions imaged in left bottom panels and middle and right bottom panels, respectively. Representative pictures of an invasive carcinoma with irregular glandular architecture, gland in gland formation (white arrowhead) and luminal debris (asterisk). Mitotic figures are encountered (arrows) and there is high proliferative activity (Ki67). Invasion of isolated or small aggregates of cells into the stroma is observed (black arrowheads). $n = 13$ mice. Scale bars, 100 μm.

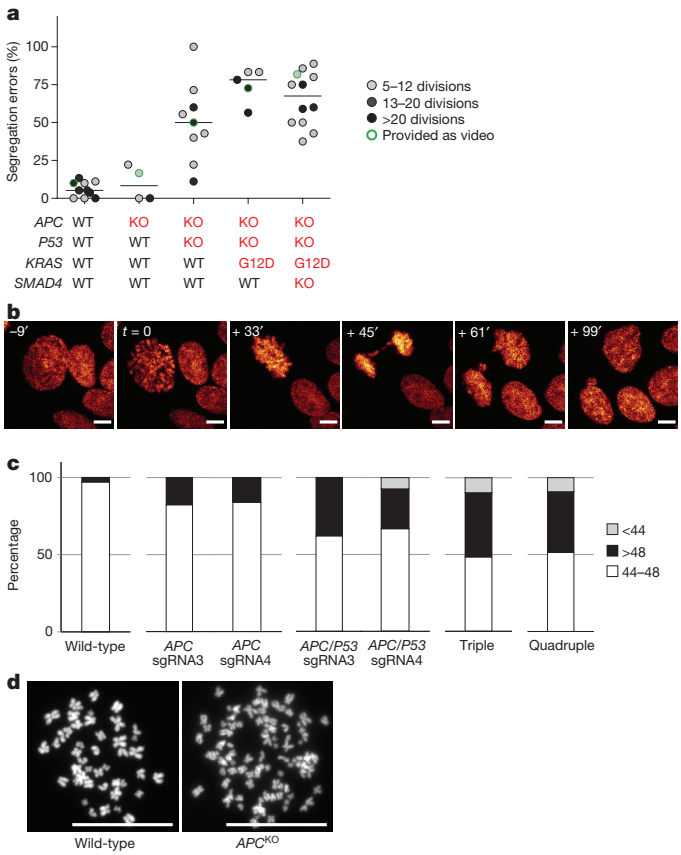

Figure 4 | Progressive CIN and aneuploidy upon introduction of CRC mutations. **a**, Live-cell imaging was performed to monitor chromosome segregations. Graph shows the percentage of erroneous mitoses. Each dot represents the percentage of errors in one organoid. Horizontal bars represent median of all dots. Videos are included of organoids depicted as dots with green outline (Supplementary Videos 1–5). WT, wild-type; KO, knockout. **b**, Stills of a typical erroneous mitotic event (anaphase bridge) in an $APC^{KO}/P53^{KO}$ organoid. Time points are indicated in minutes relative to prophase onset. Scale bars, 5 μm. **c**, Chromosomes were counted in the indicated organoids. Graphs plot the percentage of cells with chromosome counts <44, 44–48 (normal) and >48 (at least 50 spreads were counted). **d**, Representative karyotypes of a wild-type culture with $n = 46$ chromosomal counts (left) and APC^{KO} organoid culture (right) with aberrant chromosome numbers. Scale bars, 25 μm.

using three-dimensional live-cell imaging. Wild-type organoids underwent mitosis without showing any major abnormalities. We did not observe an increase in the percentage of errors in APC^{KO} organoids (Fig. 4a and Supplementary Videos 1 and 2). However, $APC^{KO}/P53^{KO}$ organoids showed a progressive increase in the percentage of errors. We mainly observed anaphase bridges, but a few misaligned and lagging chromosomes were also detected (Fig. 4a, b and Supplementary Video 3). Importantly, compared to $APC^{KO}/P53^{KO}$ organoids, triple and quadruple mutants showed only a minor increase in the percentage of mitotic errors (Fig. 4a and Supplementary Videos 3–5), implying that loss of *APC* and *P53* is sufficient to acquire CIN.

To verify that the observed CIN results in aneuploidy, we next counted chromosome numbers. Unlike wild-type organoids, karyotyping reproducibly revealed numerical aberrations in a low percentage of APC^{KO} organoids (two independent sgRNAs) (Fig. 4c, d). This ranged from a trisomy of chromosome 7 to near-tetraploid metaphases (Extended Data Fig. 6a), the latter confirming previous studies in mouse embryonic stem cells[23]. Strikingly, one of the most recurrent chromosomal aberrations in low-grade colorectal adenomas in patients involves copy number gains of chromosome 7 (refs 24–26). In accordance with the chromosome segregation analyses, $APC^{KO}/P53^{KO}$ organoids showed a marked increase in the percentage of aneuploid spreads (Fig. 4c and Extended Data Fig. 6b). The triple and quadruple mutants also showed extensive aneuploidy (Fig. 4c and Extended Data Fig. 6c, d).

To confirm these data, APC^{KO}, $P53^{KO}$ and $APC^{KO}/P53^{KO}$ organoids were engineered in a second human small intestinal line (Extended Data Fig. 7a–c). Again, loss of both *APC* and *P53* had the most dramatic effect on CIN and aneuploidy. Although the single loss of *P53* resulted in a substantial increase in the percentage of segregation errors, only a minor increase in the amount of aberrant spreads was observed (Extended Data Fig. 7d, f and Supplementary Video 6). Thus, we show that the combined loss of *APC* and *P53* is

sufficient for the appearance of extensive aneuploidy. Despite the observed chromosome missegregations, our engineered lines continue proliferating, while maintaining functional DNA damage signalling (Extended Data Fig. 7h).

CRC mutations in human colon organoids

Finally, we introduced all the mutation combinations described earlier into a human colon organoid stem cell culture[27], following the same functional selection procedures (Extended Data Fig. 3 and Extended Data Table 1b). Importantly, this yielded essentially identical results to those obtained with the small intestinal stem cells, in terms of growth factor independence, *in vitro* appearance, CIN and aneuploidy (Extended Data Figs 5b and 7e, g). Moreover, both triple- and quadruple-mutant human colon organoids grew with high efficiency as tumours upon xenotransplantation into immunodeficient mice (Extended Data Fig. 8a, b). Histological analysis revealed that triple-mutant tumours contained large cysts and locally displayed features of well-differentiated carcinomas with relatively limited invasive growth, whereas the quadruple-mutant-derived invasive carcinomas were faster growing, had a poorly differentiated appearance and displayed very frequent tumour budding at the invasive front, as well as invasion of the underlying muscle tissue (Extended Data Fig. 8c–e).

While this manuscript was under final review, a study using a similar strategy appeared[28]. Our CRC progression model selects out functional mutants by changing the culture medium composition and all sgRNAs were designed to target mutation hotspot regions. Therefore, we believe that our model reflects the *in vivo* situation more closely than any other *in vitro* human CRC model so far. Upon oncogenic mutation of *KRAS*, *APC*, *P53* and *SMAD4*, human gut stem cell organoids can grow in the absence of all stem-cell-niche factors and in the presence of the P53 stabilizer nutlin-3 *in vitro* and as tumours with invasive carcinoma features *in vivo*. Moreover, we find that our engineered CRC organoid lines show marked CIN and aneuploidy, both considered to be hallmarks of cancer[22].

Online Content Methods, along with any additional Extended Data display items and Source Data, are available in the online version of the paper; references unique to these sections appear only in the online paper.

Received 11 November 2014; accepted 16 March 2015.
Published online 29 April 2015.

1. Fearon, E. R. & Vogelstein, B. A genetic model for colorectal tumorigenesis. *Cell* **61,** 759–767 (1990).
2. Fearon, E. R. Molecular genetics of colorectal cancer. *Annu. Rev. Pathol.* **6,** 479–507 (2011).
3. The Cancer Genome Atlas Network. Comprehensive molecular characterization of human colon and rectal cancer. *Nature* **487,** 330–337 (2012).
4. Barker, N. *et al.* Crypt stem cells as the cells-of-origin of intestinal cancer. *Nature* **457,** 608–611 (2009).
5. Schepers, A. G. *et al.* Lineage tracing reveals Lgr5$^+$ stem cell activity in mouse intestinal adenomas. *Science* **337,** 730–735 (2012).
6. Zhu, L. *et al.* Prominin 1 marks intestinal stem cells that are susceptible to neoplastic transformation. *Nature* **457,** 603–607 (2009).
7. Li, X. *et al.* Oncogenic transformation of diverse gastrointestinal tissues in primary organoid culture. *Nature Med.* **20,** 769–777 (2014).
8. Sato, T. *et al.* Single Lgr5 stem cell build crypt-villus structures *in vitro* without a mesenchymal niche. *Nature* **459,** 262–265 (2009).
9. Sato, T. *et al.* Long-term expansion of epithelial organoids from human colon, adenoma, adenocarcinoma, and Barrett's epithelium. *Gastroenterology* **141,** 1762–1772 (2011).
10. Sato, T. & Clevers, H. Primary mouse small intestinal epithelial cell cultures. *Methods Mol. Biol.* **945,** 319–328 (2013).
11. Jung, P. *et al.* Isolation and *in vitro* expansion of human colonic stem cells. *Nature Med.* **17,** 1225–1227 (2011).
12. Huch, M. *et al.* Unlimited *in vitro* expansion of adult bi-potent pancreas progenitors through the Lgr5/R-spondin axis. *EMBO J.* **32,** 2708–2721 (2013).
13. Huch, M. *et al. In vitro* expansion of single Lgr5$^+$ liver stem cells induced by Wnt-driven regeneration. *Nature* **494,** 247–250 (2013).
14. Mali, P. *et al.* RNA-guided human genome engineering via Cas9. *Science* **339,** 823–826 (2013).
15. Cho, S. W., Kim, S., Kim, J. M. & Kim, J. S. Targeted genome engineering in human cells with the Cas9 RNA-guided endonuclease. *Nature Biotechnol.* **31,** 230–232 (2013).
16. Cong, L. *et al.* Multiplex genome engineering using CRISPR/Cas systems. *Science* **339,** 819–823 (2013).
17. Schwank, G. *et al.* Functional repair of CFTR by CRISPR/Cas9 in intestinal stem cell organoids of cystic fibrosis patients. *Cell Stem Cell* **13,** 653–658 (2013).
18. Vassilev, L. T. *et al. In vivo* activation of the p53 pathway by small-molecule antagonists of MDM2. *Science* **303,** 844–848 (2004).
19. Shi, Y., Hata, A., Lo, R. S., Massaqué, J. & Pavletich, N. P. A structural basis for mutational inactivation of the tumour suppressor Smad4. *Nature* **388,** 87–93 (1997).
20. Chacko, B. M. *et al.* Structural basis of heteromeric smad protein assembly in TGF-β signaling. *Mol. Cell* **15,** 813–823 (2004).
21. Fleming, N. I. *et al. SMAD2*, *SMAD3* and *SMAD4* mutations in colorectal cancer. *Cancer Res.* **73,** 725–735 (2013).
22. Rajagopalan, H., Nowak, M. A., Vogelstein, B. & Lengauer, C. The significance of unstable chromosomes in colorectal cancer. *Nature Rev. Cancer* **3,** 695–701 (2003).
23. Fodde, R. *et al.* Mutations in the *APC* tumour suppressor gene cause chromosomal instability. *Nature Cell Biol.* **3,** 433–438 (2001).
24. Bomme, L. *et al.* Clonal karyotypic abnormalities in colorectal adenomas: clues to the early genetic events in the adenoma-carcinoma sequence. *Genes Chromosom. Cancer* **10,** 190–196 (1994).
25. Herbergs, J. *et al.* Chromosome aberrations in adenomas of the colon. Proof of trisomy 7 in tumor cells by combined interphase cytogenetics and immunocytochemistry. *Int. J. Cancer* **57,** 781–785 (1994).
26. Ried, T. *et al.* Comparative genomic hybridization reveals a specific pattern of chromosomal gains and losses during the genesis of colorectal tumors. *Genes Chromosom. Cancer* **15,** 234–245 (1996).
27. Van de Wetering, M. *et al.* Prospective derivation of a Living Organoid Biobank of colorectal cancer patients. *Cell* http://dx.doi.org/10.1016/j.cell.2015.03.053 (in the press).
28. Matano, M. *et al.* Modelling colorectal cancer using CRISPR-Cas9-mediated engineering of human intestinal organoids. *Nature Med.* **21,** 256–262 (2015).

Supplementary Information is available in the online version of the paper.

Acknowledgements We would like to thank H. M. Rodermond for help with *in vivo* transplantation assays and members of the contributing laboratories for support. We thank A. Pronk, W. van Houdt and J. van Gorp for facilitating human colon tissue. We are grateful for support from the following: The Netherlands Organisation for Scientific Research (NWO-ZonMw) VENI grant to J.D. (91614138); University of Amsterdam (2012-5735) and The Dutch Digestive Diseases Foundation (MLDS) (FP13-07) to C.Z. and J.P.M.; Netherlands Institute of Regenerative Medicine (N.S. and G.S.); Dutch Cancer Society (KWF) (KWF/PF-HUBR 2007-3956 for H.B.; KWF Fellowship UU2013-6070 for H.J.S.); Stand Up to Cancer/Stichting Vrienden van het Hubrecht (M.v.d.W.); NWO-ZonMw (116.005.002 for R.v.B.); and the CancerGenomics.nl (NWO Gravitation) program.

Author Contributions J.D. and H.C. conceived the project and wrote the manuscript. J.D. engineered and characterized all mutant organoid lines. R.H.v.J., B.P., H.J.S., R.M.O. and G.J.P.L.K. designed and performed live-cell imaging experiments. C.Z. and J.P.M. performed *in vivo* transplantation assays. R.v.B. and E.C. performed off-target analyses. J.D. performed karyotyping. A.B. made karyograms. G.J.O. staged subcutaneous tumours. H.B. and J.K. performed immunohistochemistry. N.S. optimized matrix for organoid growth. G.S. designed *APC* sgRNAs. M.v.d.W. established normal human colon organoid line. M.L. helped genotype the mutant small intestinal organoids.

Author Information Sequencing data have been deposited in the EMBL European Nucleotide Archive under accession number ERP009240. Reprints and permissions information is available at www.nature.com/reprints. The authors declare no competing financial interests. Readers are welcome to comment on the online version of the paper. Correspondence and requests for materials should be addressed to H.C. (h.clevers@hubrecht.eu).

METHODS

Human material for organoid cultures. Approval for this study was obtained by the ethics committees of the University Medical Centre Utrecht (duodenal biopsies) and The Diakonessen Hospital Utrecht (colonic tissues). Written informed consent was obtained.

Organoid culture. Endoscopic duodenal biopsy samples were obtained from two female individuals (patient 1, age 2 years; patient 2, age 8 years). These individuals were admitted for suspected coeliac disease or dyspepsia. Upon immunological and pathophysiological analysis, none of the individuals was diagnosed with coeliac disease, whereas patient 1 presented with signs of gastric metaplasia. All duodenal biopsies that were used in this study were found to be healthy on the basis of histological examination. Normal human colon tissue was isolated from a resected colon segment derived from a patient (female, age 60 years) diagnosed with CRC (sigmoid). Culture establishment was described previously[17,27]. Culture medium contains advanced DMEM/F12 medium (Invitrogen) including B27 (Invitrogen), nicotinamide (Sigma-Aldrich), *N*-acetylcysteine (Sigma-Aldrich), noggin (Peprotech), R-spondin 1 (ref. 29), EGF (Peprotech), WNT conditioned media (50%, produced using stably transfected L cells), TGF-β type I receptor inhibitor A83-01 (Tocris) and P38 inhibitor SB202190 (Sigma-Aldrich). For selection of $KRAS^{G12D}$ mutants, organoids were grown in culture medium lacking EGF and containing 0.5–1.0 μM of gefitinib (Selleck Chemicals). For mutant *P53* selection, organoids were cultured in the presence of 5–10 μM nutlin-3 (Cayman Chemical). Organoids were repeatedly tested for mycoplasma contamination and resulted negative.

Organoid transfection and genotyping. The organoid lipofection protocol was previously described in detail[17]. In short, human organoids were grown in the media described earlier, and trypsinized for 10 min at 37 °C. After trypsinization, cells were resuspended in 450 μl growth medium (containing the Rho kinase inhibitor Y-27632) and plated in 48-well plates at high density (80–90% confluent). Nucleic acid–Lipofectamine 2000 complexes were prepared according to the standard Lipofectamine 2000 protocol (Invitrogen). Four microlitres of Lipofectamine 2000 reagent in 50 μl Opti-MEM medium (Gibco), and a total of 1.5 μg of DNA (sgRNA, Cas9, with/without oligonucleotide in 50 μl Opti-MEM medium) were mixed together, incubated for 5 min, and added to the cells (50 μl per well). The plate was centrifuged at 600*g* at 32 °C for 1 h, and incubated for 4 h at 37 °C before single cells were plated in Basement Membrane Extract (BME; Amsbio) or Matrigel (BD Biosciences). Growth medium plus Y-27632 was exchanged with selection medium 3 days after transfection. For clonal expansion single organoids were picked. On average, the efficiency of introduction of frame-shift-inducing mutations was approximately 1%. sgRNA transfections and subsequent selections were performed at least three times in both human small intestine and colon lines.

For genotyping, genomic DNA was isolated using Viagen Direct PCR (Viagen). Primers for the PCR amplification using GoTaq Flexi DNA polymerase (Promega) were as follows: *APC*_for, 5′-TGTAATCAGACGACACAGGAAG CAGA-3′, *APC*_rev, 5′-TGGACCCTCTGAACTGCAGCAT-3′; *P53*_for, 5′-CAGGAAGCCAAAGGGTGAAGA-3′, *P53*_rev, 5′-CCCATCTACAGTCCCC CTTG-3′; *KRAS*_for, 5′-TGGACCCTGACATACTCCCA-3′, *KRAS*_rev, 5′-AAGCGTCGATGGAGGAGTTT-3′; *SMAD4*_for, 5′-TGGAGTGCAAGTGA AAGCCT-3′, *SMAD4*_rev, 5′-ACCGACAATTAAGATGGAGTGCT-3′. Products were cloned into pGEM-T Easy vector system I (Promega) and subsequently sequenced using T7 sequencing primer.

Vector construction. The human codon-optimized Cas9 expression plasmid was obtained from Addgene (41815). The sgRNA-GFP plasmid was obtained from Addgene (41819) and used as a template for generating target-specific sgRNAs. The GFP targeting sequence was exchanged by inverse PCR followed by DpnI digestion and T4 ligation as described previously[17]. *APC*, *P53* and *SMAD4* sgRNA sequences are included in Extended Data Figs 1a and 2d. *KRAS* target sequences: number 1, 5′-GAATATAAACTTGTGGTAGTTGG-3′; number 2, 5′-GTAGTTGGAGCTGGTGGCGTAGG-3′.

RNA isolation, cDNA preparation and qRT–PCR. Organoids were harvested in RLT lysis buffer and RNA was isolated using the Qiagen RNeasy kit (Qiagen) according to the manufacturer's instructions. Extracted RNA was used as a template for cDNA production using GoScript reverse transcriptase (Promega) according to the manufacturer's protocol. qRT–PCR was performed using IQ SYBR green mix (Bio-Rad) according to the manufacturer's protocol. Results were calculated by using the ΔΔCt method. Organoid treatments: WNT/R-spondin withdrawal, 48 h; nutlin-3 10 μM, 24 h. Primer sequences: *AXIN2*_for, 5′-AGCTTACATGAGTAATGGGG-3′, *AXIN2*_rev, 5′-AATTCCATCTACACTG CTGTC-3′; *P21*_for, 5′-TACCCTTGTGCCTCGCTCAG-3′, *P21*_rev, 5′-GAGAAGATCAGCCGGCG TTT-3′; *GAPDH*_for, 5′-TGCACCACCAACTG CTTAGC-3′, *GAPDH*_rev, 5′-GGCATGGACTGTGGTCATGAG-3′.

Western blot. Samples were lysed using RIPA buffer (50 mM Tris-HCl pH 8.0, 150 mM NaCl, 0.1% SDS, 0.5% Na-Deoxycholate, 1% NP-40) containing Complete protease inhibitors (Roche). Protein content was quantified using standard Bradford assay (BioRad) and equal amounts of protein were run on SDS–PAGE gels and transferred to PVDF membranes (Millipore). For APC western blotting, protein lysates were loaded on gradient polyacrylamide gels (4–15%; BioRad) and subsequently transferred. Membranes were blocked and probed with antibodies directed against P53 (DO-1, Santa Cruz Biotechnology), P21 (F-5, Santa Cruz Biotechnology), APC (FE9, Calbiochem), SMAD4 (B8, Santa Cruz Biotechnology), phospho-Chk1 Ser 345 (Bioke) and GAPDH (ab-9485, Abcam). Organoid treatments: nutlin-3 10 μM, 24 h; doxorubicin 10 μM, overnight. Uncropped versions of the most relevant images are provided in Supplementary Fig. 1.

***In vivo* transplantation assays.** Approval for this study was obtained by the Animal Experimentation Committee at the Academic Medical Centre in Amsterdam (DEC102581). Human organoid lines were expanded in their corresponding selection media and trypsinized for 10 min at 37 °C. After trypsinization, 200,000 cells were resuspended in 50 μl of medium containing 2× required growth factors, mixed with Matrigel (BD Biosciences) at a 1:1 ratio and injected subcutaneously into NOD scid gamma (NSG; NOD.Cg-Prkdc^{scid} Il2rg^{tm1Wjl}/SzJ) mice (≥6 injections per organoid line). After 7 (colon) or 8 (small intestine) weeks, mice were killed and nodules were processed for analysis. Both males and females (aged 8–10 weeks at the start of the experiment; weights, ~30 g for males and ~25 g for females) were used. This was randomly distributed and does not affect outgrowth. All animals were included in the analysis. Ear clipping was used for animal recognition. Number of injections was chosen following previous experience in the assessment of experimental variability. Animals were caged together and treated in the same way.

Immunohistochemistry. Tissues were fixed in 4% paraformaldehyde, dehydrated and embedded in paraffin. Sections were subjected to H&E as well as immunohistochemical staining. The following primary antibodies were used for immunohistochemical staining: anti-cytokeratin clone Cam5.2 (BD Biosciences), anti-Ki67 clone MM1 (Sanbio) and E-cadherin clone 36 (BD Biosciences).

Live-cell imaging and karyotyping. To visualize mitoses, organoids were infected with lentivirus encoding mNeon-tagged histone 2B and a puromycin-resistance cassette (pLV-H2B-mNeon-ires-Puro)[30]. After two passages, these were plated in BME in glass-bottom 96-well plates and mounted on an inverted confocal laser scanning microscope (Leica SP8X), which was continuously held at 37 °C and equipped with a culture chamber for overflow of 6.0% CO_2. Over 16–20 h, ~10 H2B-mNeon-expressing organoids were imaged simultaneously in XYZT-mode using a ×40 objective (N.A. 1.1), using minimal amounts of 506 nm laser excitation light from a tuneable white light laser. Time interval was approximately 3 min (2:30–3:20 min). For post-acquisition analyses of mitotic behaviour, data sets were converted into manageable and maximally informative videos, combining *z*-projection, depth colour-coding and merging with transmitted light images (Supplementary Videos 1–6). Mitoses were scored, judged and counted manually.

For karyotyping, organoids were treated with 0.1 μg ml^{-1} colcemid (Gibco) for 16 h. Cultures were washed and dissociated into single cells using TrypLE (Gibco) and processed as described[13]. Slides were mounted with DAPI-containing vectashield and analysed on a DM6000 Leica microscope (at least 50 spreads were analysed, $n = 3$).

Off-target effect analysis. To assess off-target mutational effects, we computationally identified candidate off-target sites for each sgRNA using COD software (http://cas9.wicp.net/). The software calculates an off-target score depending on sequence similarity: if the sequence perfectly matches the tested sgRNA (the target site) the score is 1 and decreases with increasing sequence differences. For the sgRNA targeting *P53* and *SMAD4* we identified 2 and 11 candidate off-target sites (Supplementary Table 1). For the sgRNA targeting *APC* and *KRAS* we only considered sites with an off-target scores of at least 0.15 or higher, resulting in 74 and 15 candidate off-target sites, respectively. We evaluated off-target mutational effects by amplicon-based NGS sequencing 93 candidate off-target sites and included the target sites for *P53*, *KRAS* and *SMAD4* as positive controls (Supplementary Table 1). To this end, primers were designed ~350 nucleotides 5′ and ~150 nucleotides 3′ from the candidate site to obtain amplicons of ~500 bp (primer sequences available upon request). These regions were PCR amplified for each of the cultures using 5 ng genomic DNA, 1× GoTaq PCR Buffer (Promega), 1.5 mM $MgCl_2$, 0.2 mM of each dNTP, 0.2 mM of each primer of a primer pair and 0.25 units of GoTaq polymerase (Promega) in a final volume of 10 ml at 94 °C for 60 s; 15 cycles at 92 °C for 30 s, 65 °C for 30 s with a decrement of 0.2 °C per cycle and 72 °C for 60 s; followed by 30 cycles at 92 °C for 30 s, 58 °C for

30 s and 72 °C for 60 s; and a final extension at 72 °C for 180 s. Per culture the PCR products were pooled and barcoded. Illumina sequence libraries were generated using the TruSeq DNA Sample Preparation Kit (Illumina) according to the manufacturer's protocol. Subsequently, the libraries were pooled and sequenced using the MiSeq sequencer (2 × 250 bp) to a depth of >10,000× base coverage. Sequence reads were mapped to the human reference genome (GRCh37/hg19), using the Burrows–Wheeler Aligner (BWA) Maximal Exact Matches (MEM) v.0.7.5a mapping tool[31] with settings '-c 100 -m'. Small indel calling was performed using the Genome Analysis Toolkit (GATK)[32] haplotype caller v.3.2-2 with 'best practices' settings. We only considered indels with a variant allele frequency (VAF) of at least 0.15 or higher (Supplementary Table 1).

29. Kim, K. A. *et al.* Mitogenic influence of human R-spondin1 on the intestinal epithelium. *Science* **309,** 1256–1259 (2005).
30. Shaner, N. C. *et al.* A bright monomeric green fluorescent protein derived from Branchiostoma lanceolatum. *Nature Methods* **10,** 407–409 (2013).
31. Li, H. & Durbin, R. Fast and accurate short read alignment with Burrows–Wheeler transform. *Bioinformatics* **25,** 1754–1760 (2009).
32. DePristo, M. A. *et al.* A framework for variation discovery and genotyping using next-generation DNA sequencing data. *Nature Genet.* **43,** 491–498 (2011).

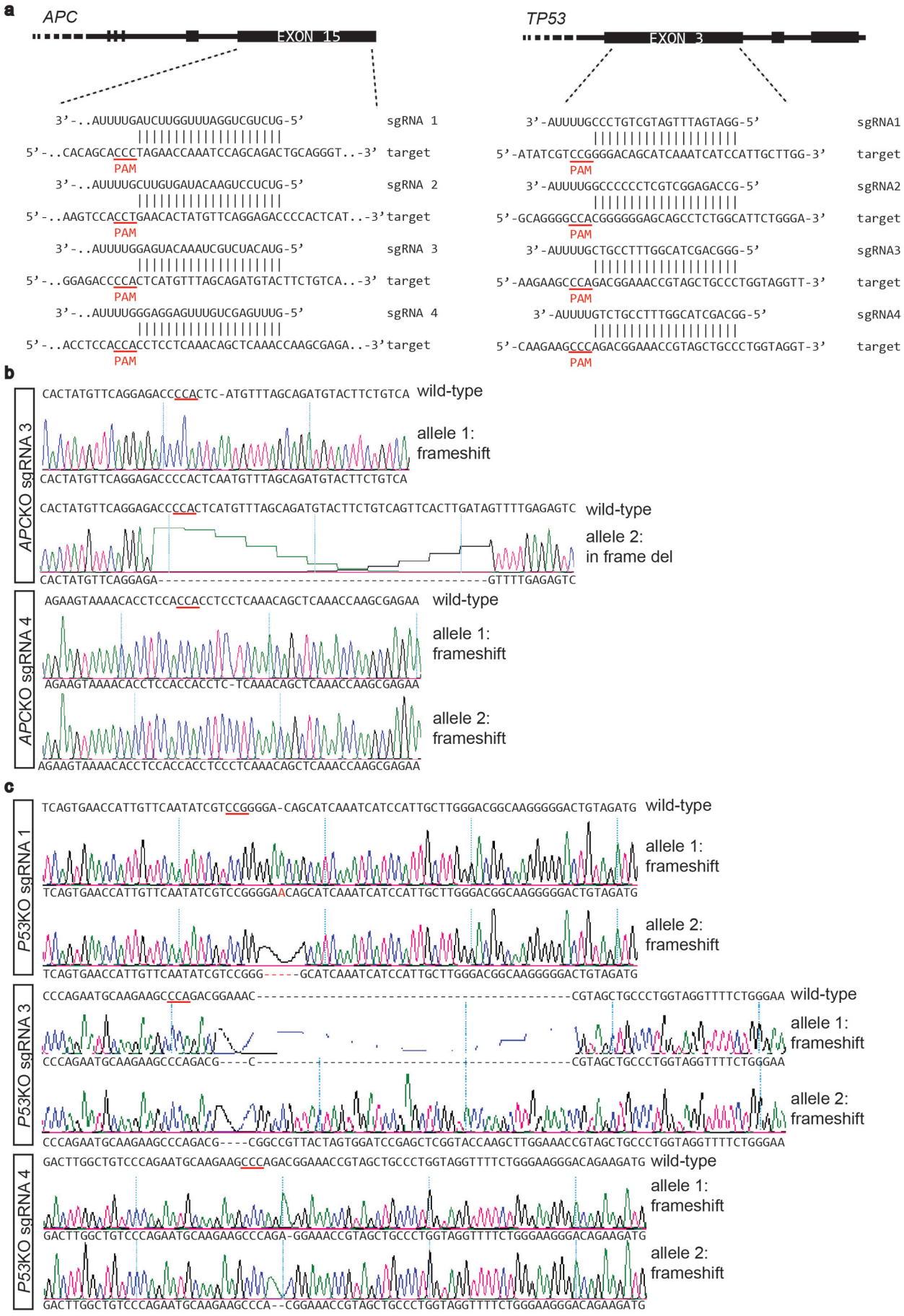

Extended Data Figure 1 | Introducing inactivating mutations in the *APC* and *P53* genes in human intestinal organoids using CRISPR/Cas9. **a**, Schematic representation of the targeted exon of the human *APC* (left) and *P53* (right) loci and sequences of the designed sgRNAs. **b**, **c**, PCR amplification products of the mutated alleles of *APC* (**b**) and *P53* (**c**) were obtained using primers flanking the targeted exon. Subsequent sequencing revealed indels at the expected locations. PAM sequences are underlined in red in wild-type sequences. Of note, the curved lines bridging the gaps in deleted alleles are drawn by the alignment software.

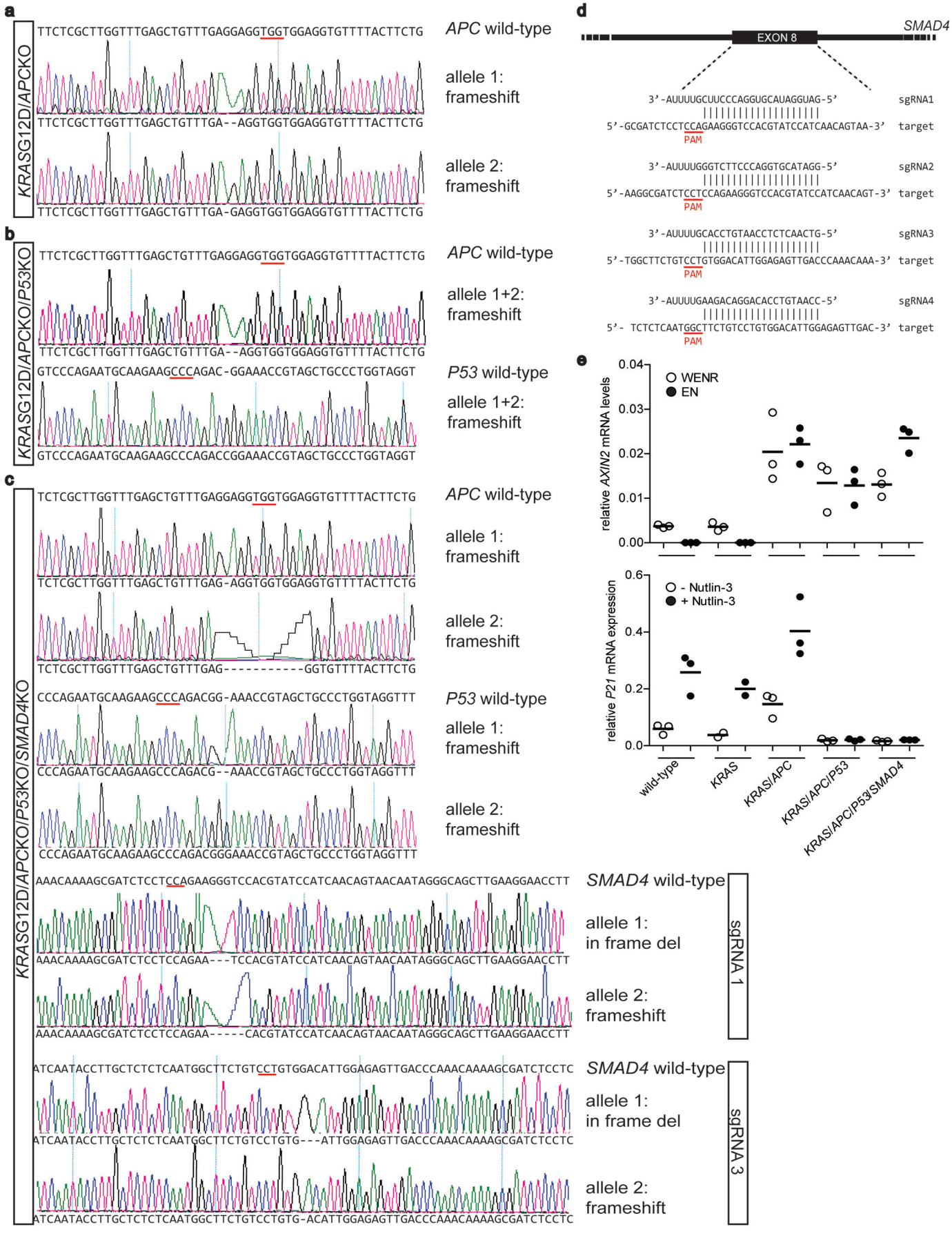

Extended Data Figure 2 | *KRAS*^{G12D}, *APC*^{KO}, *P53*^{KO} and *SMAD4*^{KO} mutation combinations in human intestinal organoids. **a**–**c**, PCR amplification products of the indicated genes of *KRAS*^{G12D}/*APC*^{KO} (**a**), *KRAS*^{G12D}/*APC*^{KO}/*P53*^{KO} (**b**) and *KRAS*^{G12D}/*APC*^{KO}/*P53*^{KO}/*SMAD4*^{KO} (**c**) organoids were obtained using primers flanking the targeted exon. Subsequent sequencing revealed indels at the expected locations. PAM sequences are underlined in red. Of note, the curved lines bridging the gaps in deleted alleles are drawn by the alignment software. **d**, Schematic representation of the targeted exon of the human *SMAD4* locus and sequences of the designed sgRNAs. **e**, qRT–PCR for *AXIN2* (top) and *P21* (bottom) in the indicated organoid cultures. Top, the indicated organoid lines were cultured in the presence (WENR) or absence (EN) of WNT/R-spondin. Bottom, the indicated organoid lines were cultured in the presence or absence of nutlin-3 for 24 h. Expression was normalized to *GAPDH*. Horizontal bars represent mean of $n = 3$ independent experiments.

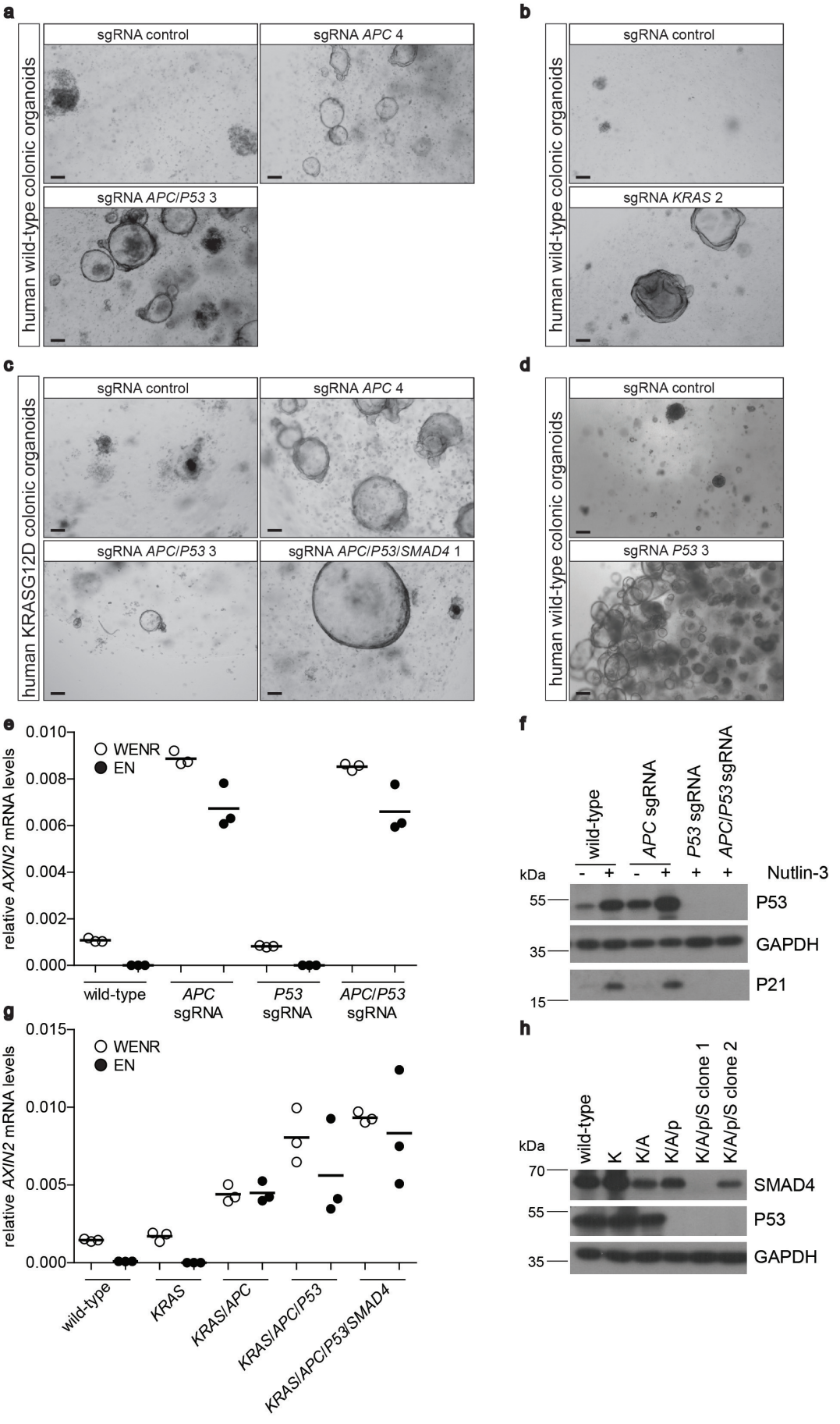

Extended Data Figure 3 | Using CRISPR/Cas9-mediated genome editing to introduce *APC, P53, KRAS*^{G12D} and *SMAD4* mutations in human colonic organoids. **a**–**d**, Using the strategies depicted in Figs 1a and 2a, d, *APC*^{KO}, *APC*^{KO}/*P53*^{KO} (**a**), *KRAS*^{G12D} (**b**), *KRAS*^{G12D}/*APC*^{KO}, *KRAS*^{G12D}/*APC*^{KO}/*P53*^{KO}, *KRAS*^{G12D}/*APC*^{KO}/*P53*^{KO}/*SMAD4*^{KO} (**c**) and *P53*^{KO} (**d**) mutant human colon organoids were generated. Experiment was performed at least three independent times for each mutation. **e**, qRT–PCR for *AXIN2* in the indicated organoid lines cultured in the presence (WENR) or absence (EN) of WNT/R-spondin. Expression was normalized to *GAPDH*. Horizontal bars represent mean of $n = 3$ independent experiments. **f**, Western blot analysis of P53 and P21 expression in the indicated human colon organoid lines cultured in the presence or absence of nutlin-3. GAPDH, loading control. **g**, qRT–PCR for *AXIN2* in the indicated organoid lines cultured in the presence (WENR) or absence (EN) of WNT/R-spondin. Expression was normalized to *GAPDH*. Horizontal bars represent mean of $n = 3$ independent experiments. **h**, Western blot analysis of SMAD4 and P53 expression in the indicated human colon organoid lines. Please note that quadruple-mutant clone 1 contains *SMAD4* frameshift-inducing indels in both alleles whereas clone 2 contains a frameshift-inducing indel in one and an in-frame deletion in the other allele (reduced SMAD4 expression). GAPDH, loading control. Scale bars, 100 μm.

a

organoid line	# nodules/# injections	% outgrowth
KRAS^{G12D}/*APC*^{KO}/*P53*^{KO} (triple)	3/12	25%
KRAS^{G12D}/*APC*^{KO}/*P53*^{KO}/*SMAD4*^{KO} (quadruple)	13/16	81%

b

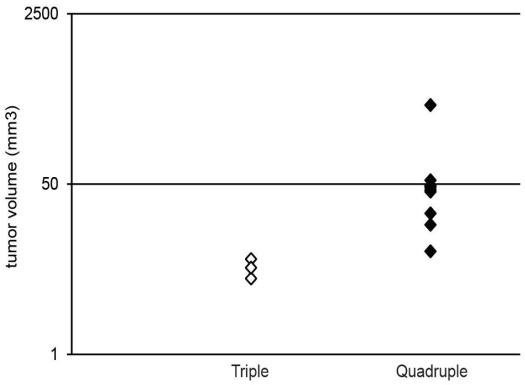

c

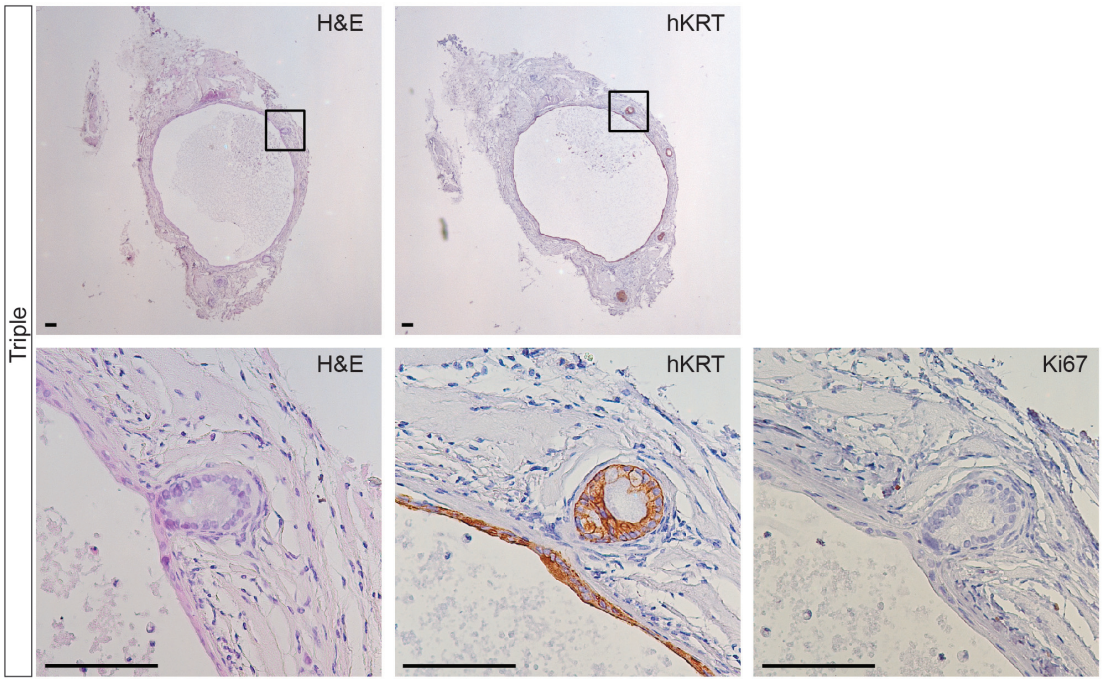

d

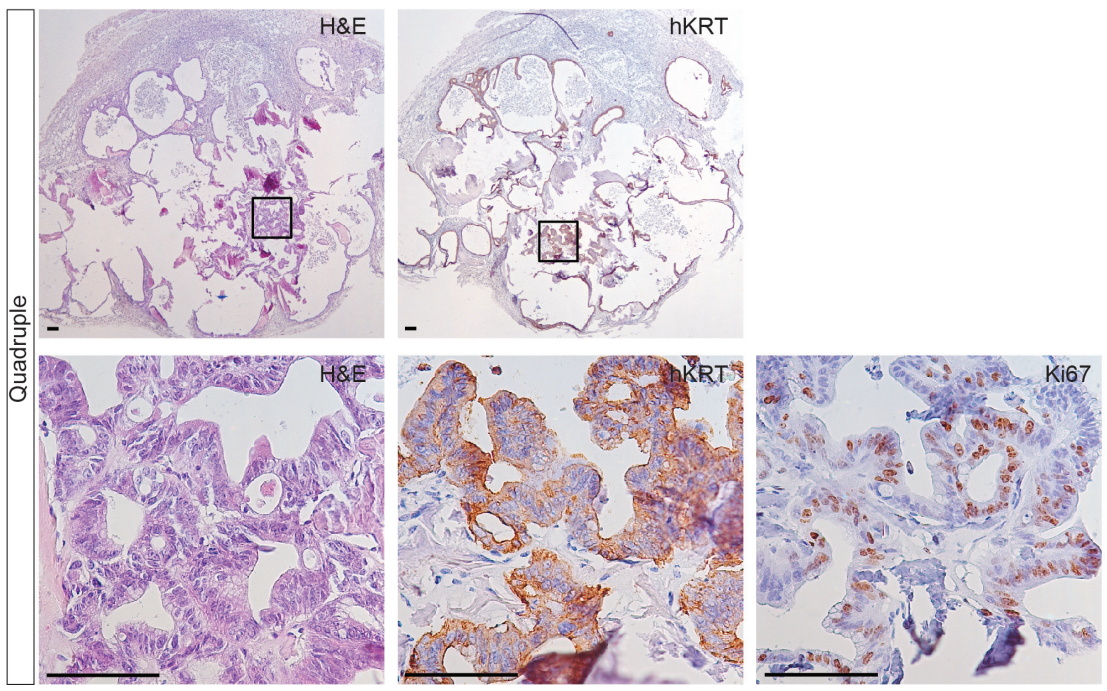

Extended Data Figure 4 | Quadruple-mutant human intestinal organoids grow as tumours with features of invasive carcinoma *in vivo*. **a**, Wild-type and all engineered human intestinal organoid lines were injected subcutaneously in immunodeficient mice. Mice injected with $KRAS^{G12D}$/APC^{KO}/$P53^{KO}$ (triple) and $KRAS^{G12D}$/APC^{KO}/$P53^{KO}$/$SMAD4^{KO}$ (quadruple) organoids developed visible nodules. **b**, Tumour sizes were examined 8 weeks after transplantation. **c**, **d**, H&E (top left, bottom left), hKRT (top right, bottom middle) and Ki67 (bottom right) immunostainings on nodules isolated from triple- (**c**) and quadruple-mutant (**d**) injected mice. Triple-mutant organoids did engraft but remained small, showed only weak proliferation and had adenoma features ($n = 3$ mice). Quadruple-mutant-derived tumours were highly proliferative with features of invasive carcinoma ($n = 13$ mice). See Fig. 3 for more details. Scale bars, 100 μm.

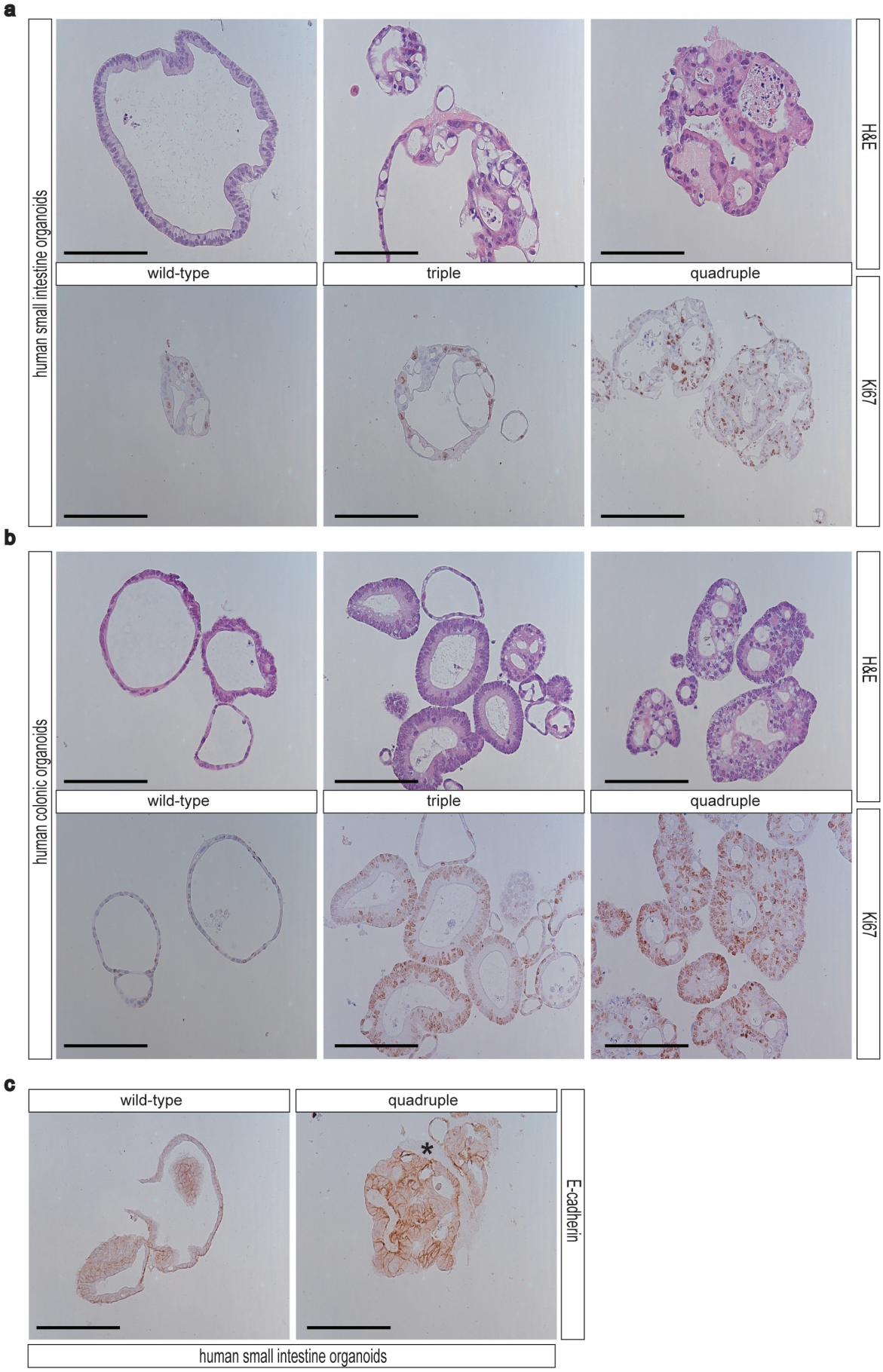

Extended Data Figure 5 | Histological analysis of triple- and quadruple-mutant organoids reveals morphological changes *in vitro*. **a**, Representative H&E and Ki67 immunostainings on the indicated human small intestinal organoid lines ($n = 4$ independent experiments). **b**, Representative H&E and Ki67 immunostainings on the indicated human colon organoid lines ($n = 3$ independent experiments). **c**, Representative E-cadherin immunostainings on wild-type and quadruple-mutant human small intestinal organoids ($n = 4$ independent experiments). Asterisk indicates residual Matrigel. Scale bars, 100 μm.

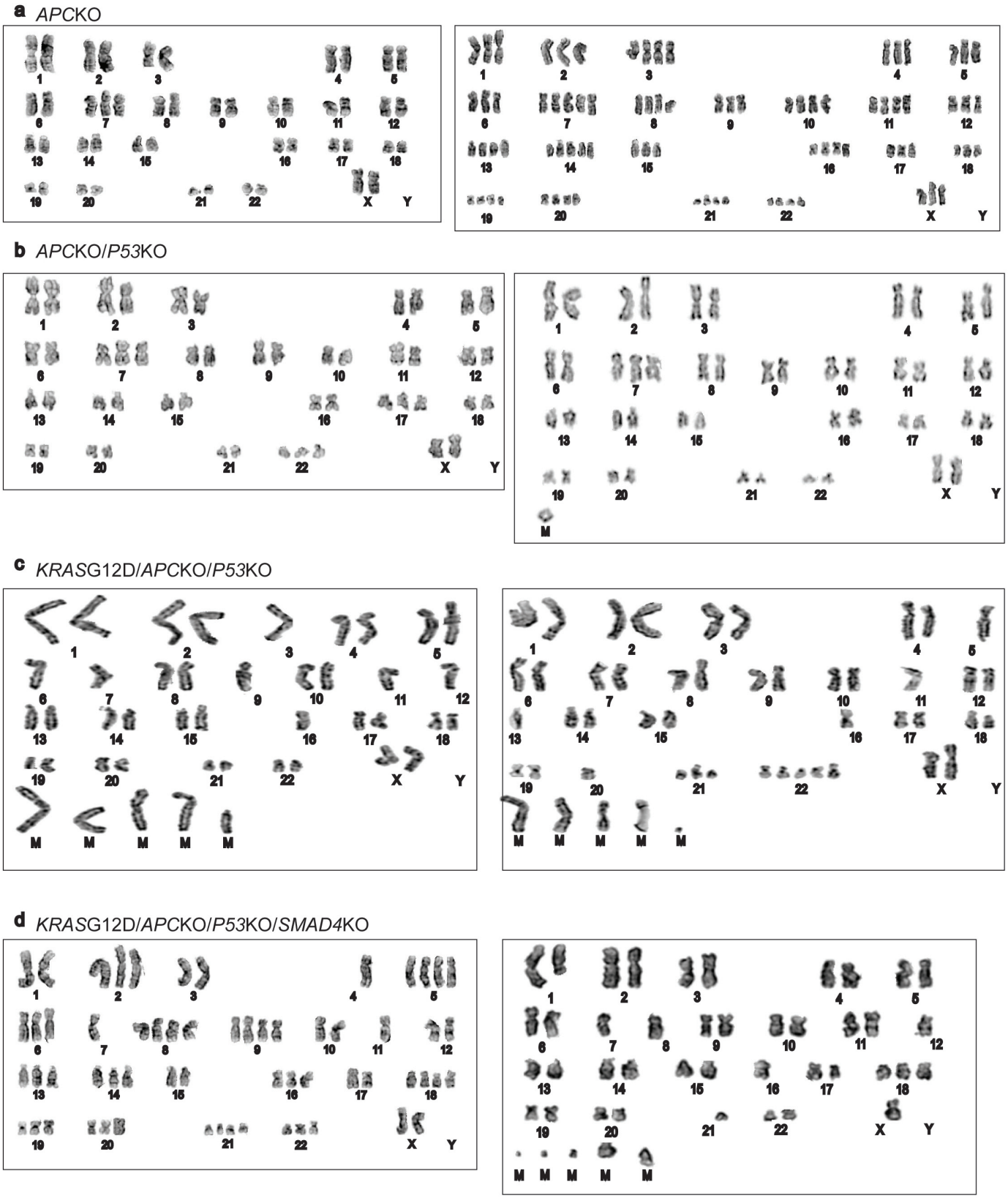

Extended Data Figure 6 | Progressive aneuploidy upon introduction of CRC mutations. **a**–**d**, Karyograms of APC^{KO} (**a**), $APC^{KO}/P53^{KO}$ (**b**), $KRAS^{G12D}/APC^{KO}/P53^{KO}$ (**c**) and $KRAS^{G12D}/APC^{KO}/P53^{KO}/SMAD4^{KO}$ (**d**) organoids, showing extensive aneuploidy in organoids harbouring CRC mutations (20 spreads were analysed per line). Note the occurrence of trisomy 7 in APC^{KO} and $APC^{KO}/P53^{KO}$ (independent clones) organoids. M, marker chromosomes.

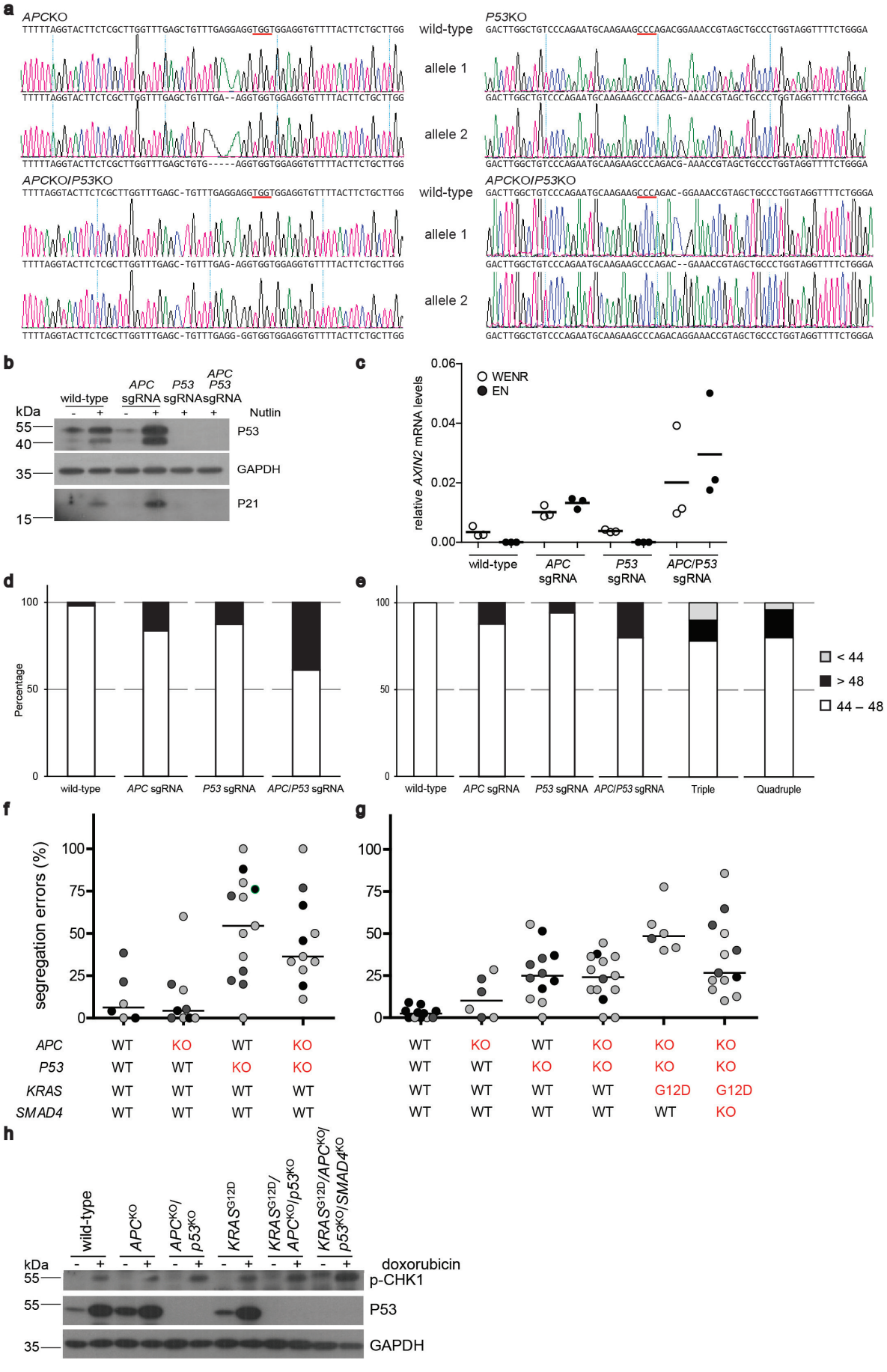

Extended Data Figure 7 | Loss of both *APC* and *P53* results in extensive CIN and aneuploidy. **a**, APC^{KO}, $P53^{KO}$ and $APC^{KO}/P53^{KO}$ mutations were introduced in a second independent human intestinal organoid line. PCR amplification products of the mutated alleles of *APC* and *P53* were obtained using primers flanking the targeted exon. Subsequent sequencing revealed frameshift-inducing indels at the expected locations. Left, *APC* genotyping; right, *P53* genotyping. PAM sequences are underlined in red. Of note, the curved lines bridging the gaps in deleted alleles are drawn by the alignment software. **b**, Western blot analysis for P53 and P21 expression in the second human intestinal organoid line cultured in the presence or absence of nutlin-3. GAPDH, loading control. **c**, qRT–PCR for *AXIN2* in the second human intestinal organoid line cultured in the presence (WENR) or absence (EN) of WNT/R-spondin. Expression was normalized to *GAPDH*. Horizontal bar represents mean of $n = 3$ independent experiments. **d**, Chromosome numbers were counted in the second human intestinal organoid lines. Graphs plot the percentage of cells with chromosome counts <44, 44–48 (normal) and >48 (at least 50 spreads were counted). **e**, As in **d**, but for indicated human colon organoid lines. **f**, Live-cell imaging was performed to monitor chromosome segregations in the indicated human small intestinal organoid lines. Graph shows the percentage of erroneous mitoses. Each dot represents the percentage of errors in one organoid. Horizontal bars represent median of all dots. A video is included of organoids depicted as dots with green outline (Supplementary Video 6). WT, wild type; KO, knockout. **g**, As in **f**, but for indicated human colon organoid lines. **h**, Western blot analysis of phospho-CHK1 and P53 expression in the indicated organoid lines treated with the DNA-damaging drug doxorubicin, or left untreated. GAPDH, loading control.

a

Human colon organoid line	# nodules/# injections
Wild-type	0/4
KRAS^{G12D}/*APC*^{KO}/*P53*^{KO} (triple)	6/6
KRAS^{G12D}/*APC*^{KO}/*P53*^{KO}/*SMAD4*^{KO} (quadruple)	8/8

b

c

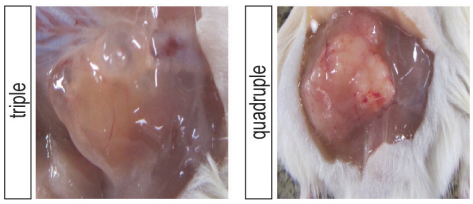

d

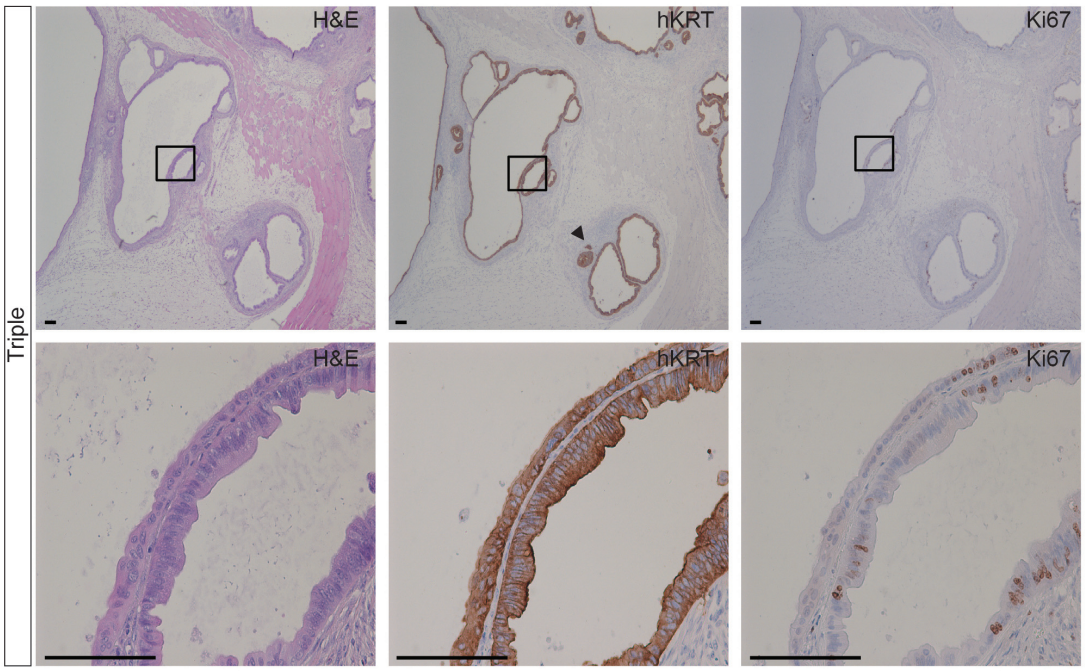

e

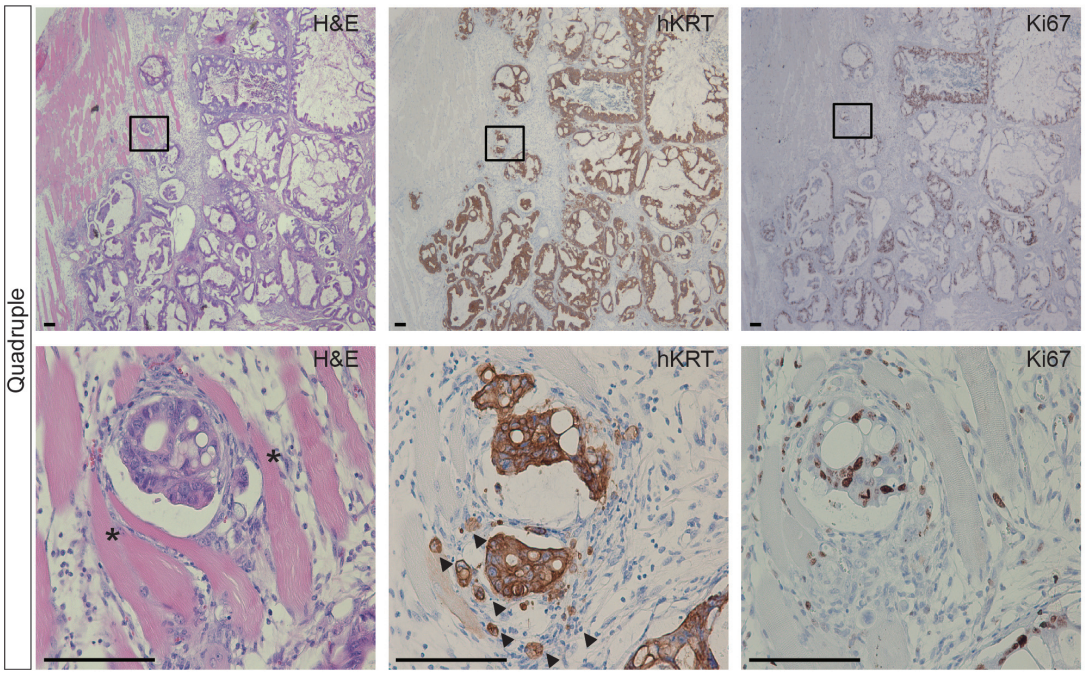

Extended Data Figure 8 | Engineered mutant human colon organoids grow as invasive carcinomas *in vivo*. **a**, Wild-type, triple- and quadruple-mutant human colon organoids were injected subcutaneously in immunodeficient mice. Nodules were counted 7 weeks after transplantation. **b**, Tumour sizes were examined 7 weeks after transplantation. **c**, Representative pictures of a 'cystic' triple-mutant (left) and 'solid' quadruple-mutant (right) tumour in immunodeficient mice. **d**, H&E (top left, bottom left), hKRT (top middle, bottom middle) and Ki67 (top right, bottom right) immunostainings on nodules isolated from triple-mutant-injected mice. Representative pictures of a well-differentiated carcinoma with limited invasive growth. The invasive growth has an expansive growth pattern with little tumour budding. $n = 6$ mice. **e**, As in **d** but for quadruple-mutant-derived tumours. Representative pictures of a poorly differentiated invasive carcinoma with frequent tumour budding at the invasive front (invasion of isolated or small aggregates of cells into the stroma is frequently observed (black arrowheads)). Invasive character is confirmed by the invasive growth into the underlying muscle tissue (asterisk, muscle tissue). $n = 8$ mice. Scale bars, 100 μm.

Extended Data Table 1 | Introducing oncogenic mutations in human intestinal organoids using CRISPR/Cas9

a

Gene targeted	Selection procedure	# of functional sgRNAs
APC	- Wnt - R-spondin	2 out of 4
P53	+ Nutlin-3	3 out of 4
KRAS	- EGF (+ gefitinib)	2 out of 2
SMAD4	- Noggin	2 out of 4

b

Organ	Organoid line	Mutation order	Genotype	*In vitro* phenotype	In vivo tumorigenicity
Small intestine	Wild-type		-	-; stable genome	No
Small intestine	APC^{KO} (sgRNA 4)	*APC*	*APC* FS_pro1443/FS_pro1443	- Wnt - R-spondin; mild aneuploidy	No
Small intestine	$APC^{KO}/P53^{KO}$ (sgRNA 4/3)	*APC>P53*	*APC* FS_pro1443/FS_pro1443 *P53* FS_phe109/FS_phe109	- Wnt - R-spondin + Nut-3; extensive aneuploidy	No
Small intestine	$KRAS^{G12D}$ (sgRNA 2)	*KRAS*	*KRAS* c.35G>A/FS_gly13	- EGF + gefitinib; N.D.	No
Small intestine	$KRAS^{G12D}/APC^{KO}$ (sgRNA 2/4)	*KRAS>APC*	*KRAS* c.35G>A/FS_gly13 *APC* FS_pro1443/FS_pro1443	- EGF - Wnt - R-spondin; N.D.	No
Small intestine	$KRAS^{G12D}/APC^{KO}/P53^{KO}$ (sgRNA 2/4/3)	*KRAS>APC, P53*	*KRAS* c.35G>A/FS_gly13 *APC* FS_pro1443/FS_pro1443 *P53* FS_phe109/FS_phe109	- EGF - Wnt - R-spondin + Nut-3; extensive aneuploidy	Adenoma
Small intestine	$KRAS^{G12D}/APC^{KO}/P53^{KO}/SMAD4^{KO}$ (sgRNA 2/4/3/1)	*KRAS>APC, P53,SMAD4*	*KRAS* c.35G>A/FS_gly13 *APC* FS_pro1443/FS_pro1443 *P53* FS_phe109/FS_phe109 *SMAD4* DEL_pro356/FS_pro356	- EGF - Wnt - R-spondin - Noggin + Nut-3; extensive aneuploidy; grow as solid tumour masses	Invasive carcinoma
Colon	Wild-type		-	-; stable genome	No
Colon	APC^{KO} (sgRNA 4)	*APC*	*APC* FS_pro1443/FS_pro1443	- Wnt - R-spondin; mild aneuploidy	N.D.
Colon	$P53^{KO}$ (sgRNA 3)	*P53*	*P53* FS_phe109/FS_phe109	+ Nut-3; mild aneuploidy	N.D.
Colon	$APC^{KO}/P53^{KO}$ (sgRNA 4/3)	*APC>P53*	*APC* FS_pro1443/FS_pro1443 *P53* FS_gly108/FS_gly108	- Wnt - R-spondin + Nut-3; extensive aneuploidy	N.D.
Colon	$KRAS^{G12D}$ (sgRNA 2)	*KRAS*	*KRAS* c.35G>A/c.35G>A	- EGF + gefitinib; N.D.	N.D.
Colon	$KRAS^{G12D}/APC^{KO}$ (sgRNA 2/4)	*KRAS>APC*	*KRAS* c.35G>A/c.35G>A *APC* FS_pro1443/FS_pro1441	- EGF - Wnt - R-spondin; N.D.	N.D.
Colon	$KRAS^{G12D}/APC^{KO}/P53^{KO}$ (sgRNA 2/4/3)	*KRAS>APC, P53*	*KRAS* c.35G>A/c.35G>A *APC* FS_pro1443/FS_pro1443 *P53* FS_phe109/FS_phe109	- EGF - Wnt - R-spondin + Nut-3; extensive aneuploidy	Well differentiated carcinoma with limited invasive growth
Colon	$KRAS^{G12D}/APC^{KO}/P53^{KO}/SMAD4^{KO}$ (sgRNA 2/4/3/1)	*KRAS>APC, P53,SMAD4*	*KRAS* c.35G>A/c.35G>A *APC* FS_pro1443/FS_pro1443 *P53* FS_gly105/FS_gly105 *SMAD4* DEL_pro356/FS_pro356	- EGF - Wnt - R-spondin - Noggin + Nut-3; extensive aneuploidy; grow as solid tumour masses	Poorly differentiated carcinoma with frequent invasive growth

a, Overview of the number of functional sgRNAs and the selection strategy used. **b**, Overview of the engineered lines. N.D., not determined.